iScience

CellPress
OPEN ACCESS

Article

Reinvestigating the clinical relevance of the m^{6}A writer METTL3 in urothelial carcinoma of the bladder

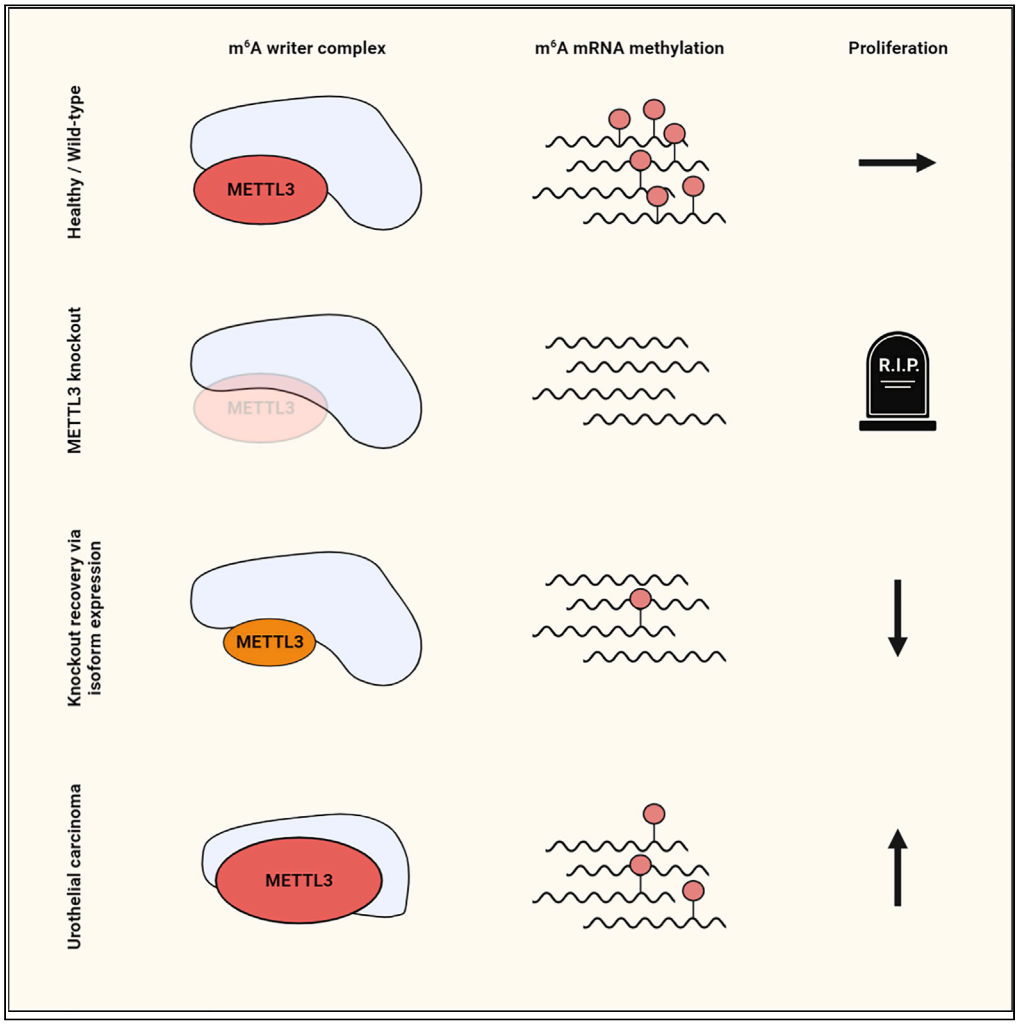

Jonas Koch, Manuel Neuberger, Martina Schmidt-Dengler, ..., Manuel Rodríguez-Paredes, Malin Nientiedt, Frank Lyko

malin.nientiedt@umm.de (M.N.)
f.lyko@dkfz.de (F.L.)

Highlights

Depletion of METTL3 reduces the oncogenic phenotype of urothelial carcinoma cells

METTL3 activity is essential for the viability of urothelial carcinoma cells

METTL3 mRNA levels do not affect the prognosis of urothelial carcinoma patients

Urothelial carcinomas display reduced overall m^{6}A mRNA levels

Koch et al., iScience 26, 107300
August 18, 2023
https://doi.org/10.1016/j.isci.2023.107300

iScience

CellPress
OPEN ACCESS

Article

Reinvestigating the clinical relevance of the m^{6}A writer METTL3 in urothelial carcinoma of the bladder

Jonas Koch,[1,5] Manuel Neuberger,[2,5] Martina Schmidt-Dengler,[3] Jinyun Xu,[1] Vitor Coutinho Carneiro,[1] Jörg Ellinger,[4] Maximilian C. Kriegmair,[2] Philipp Nuhn,[2] Philipp Erben,[2] Maurice Stephan Michel,[2] Mark Helm,[3] Manuel Rodríguez-Paredes,[1] Malin Nientiedt,[2,5,*] and Frank Lyko[1,5,6,*]

SUMMARY

METTL3 is the major writer of N6-Methyladenosine (m^{6}A) and has been associated with controversial roles in cancer. This is best illustrated in urothelial carcinoma of the bladder (UCB), where METTL3 was described to have both oncogenic and tumor-suppressive functions. Here, we reinvestigated the role of METTL3 in UCB. *METTL3* knockout reduced the oncogenic phenotype and m^{6}A levels of UCB cell lines. However, complete depletion of METTL3/m^{6}A was not achieved due to selection of cells expressing alternative METTL3 isoforms. Systematic vulnerability and inhibitor response analyses suggested that uroepithelial cells depend on METTL3 for viability. Furthermore, expression and survival analyses of clinical data revealed a complex role for METTL3 in UCB, with decreased m^{6}A mRNA levels in UCB tumors. Our results suggest that METTL3 expression may be a suitable diagnostic UCB biomarker, as the enzyme promotes UCB formation. However, the suitability of the enzyme as a therapeutic target should be evaluated carefully.

INTRODUCTION

Urothelial carcinoma of the bladder (UCB) is the fourth most common cancer disease in men with 62,420 estimated new cases, and the eight most lethal malignancy with 12,160 estimated deaths in 2023 in the United States.[1] Despite recent advances in cancer therapy, diagnostics, treatment opportunities, and five-year survival rates for UCB patients remain largely unchanged since the 1990s.[2] Thus, novel biomarkers for diagnostics and novel therapeutic drug targets are needed to improve patient prognosis.

N^6-Methyladenosine (m^{6}A) is the most abundant internal chemical modification of eukaryotic mRNAs and affects the fate of its target transcripts in terms of splicing, transport, stability or translation ratio.[3] The modification is catalyzed by a methyltransferase complex, for which METTL3 constitutes the catalytically active "writer" enzyme.[4] Furthermore, several studies demonstrated that METTL3/m^{6}A have important roles in a variety of physiological and pathophysiological processes,[5] including cellular differentiation[6,7] and cancer development.[8]

Since oncogenic roles for METTL3 were observed in multiple cancer entities,[9] the enzyme has been considered a promising therapeutic drug target. Indeed, a specific small-molecule METTL3 inhibitor decreased m^{6}A methylation levels of leukemogenic transcripts causing their translational repression, resulting in impaired engraftment and extended lifespan in a mouse leukemia model, without significant side effects.[10]

METTL3 has also been linked to UCB.[11,12] The gene is often overexpressed in UCB and m^{6}A levels were shown to be elevated 2- to 3-fold in two UCB samples compared to para-tumoral tissue.[13,14] Furthermore, high levels of METTL3 protein expression predicted shorter survival in a cohort of 180 patients, which supported the notion that METTL3 functions as an UCB oncogene.[14] Controversially, METTL3 has been also reported to have tumor-suppressive functions in UCB.[15] Therefore, the clinical potential of METTL3 for UCB patients must be evaluated carefully. Taking into account that METTL3 plays significant roles in RNA metabolism, it is also noteworthy that the loss of METTL3 leads to early embryonic lethality in

[1]Division of Epigenetics, DKFZ-ZMBH Alliance, German Cancer Research Center, 69120 Heidelberg, Germany

[2]Department of Urology and Urosurgery, Medical Faculty Mannheim, University of Heidelberg, 68167 Mannheim, Germany

[3]Institute of Pharmaceutical and Biomedical Sciences, Johannes Gutenberg-Universität, 55128 Mainz, Germany

[4]Department of Urology, University Hospital Bonn, 53127 Bonn, Germany

[5]These authors contributed equally

[6]Lead contact

*Correspondence: malin.nientiedt@umm.de (M.N.), f.lyko@dkfz.de (F.L.)

https://doi.org/10.1016/j.isci.2023.107300

mice,[7] and that *METTL3* knockout cell lines are often not viable without expressing cryptic, catalytically active isoforms of METTL3.[16] Together, these observations strongly indicate that METTL3 functions are important for viability, at least in these models.

Here, we reinvestigated the role of METTL3 in UCB and particularly focused on METTL3 viability dependencies and its clinical relevance for UCB patients. A conditional *METTL3* knockout in the UCB cell lines T24 and UM-UC-3 reduced their oncogenic phenotype, but did not result in a complete loss of m^6A levels, as selection of heterozygous cells and cells expressing aberrant METTL3 isoforms maintained a level of m^6A that supports UCB viability. Systematic vulnerability and inhibitor response analyses further supported that the majority of uroepithelial and UCB cells depend on METTL3 for viability. Expression analyses of two independent patient cohorts confirmed the upregulation of *METTL3* in UCB. However, *METTL3* expression remained stable with increasing T-stage, and survival time analyses showed that METTL3 mRNA levels do not affect the prognosis of urothelial carcinoma patients. Finally, mRNA from UCB tissue samples showed reduced global m^6A mRNA methylation levels compared to corresponding para-tumoral tissue samples, suggesting that the role of METTL3 in UCB is more complex than anticipated. Taken together, these findings have important implications for understanding the functional role of METTL3 in UCB development and reevaluating its clinical potential.

RESULTS

METTL3 depletion reduces the oncogenic phenotype of UCB cell lines

To investigate the oncogenic roles of METTL3 in UCB, we used the UCB cell lines T24 and UM-UC-3 to generate conditional knockout cells, which resulted in a strong reduction of METTL3 protein levels upon Cas9 induction (Figure 1A). *METTL3* conditional knockout cells were then subjected to different downstream analyses. METTL3 depletion led to a significant decrease in cell proliferation (T24: $p < 0.05$, UM-UC-3: $p < 0.001$, two-way analyses of variance, Figure 1B) and colony formation (T24: $p < 0.01$, UM-UC-3: $p < 0.001$, two-tailed Student's *t* test, Figure 1C), while Caspase 3/7 activity measurements suggested a significantly increased apoptosis rate (T24 and UM-UC-3: $p < 0.01$, two-tailed Student's *t* test, Figure 1D). Taken together, METTL3 depletion reduced the oncogenic phenotype in T24 and UM-UC-3 cells, which is consistent with previous findings.[14,17,18]

METTL3 activity is essential for viability in uroepithelial and UCB cells

We next isolated total RNA and mRNA fractions from our conditional *METTL3* knockout cells 24 h after induction and investigated their global m^6A methylation levels by LC-MS/MS. Global m^6A levels were significantly decreased in mRNA preparations (T24: $p < 0.01$, UM-UC-3: $p < 0.05$, two-tailed Student's *t* test, Figure 2A), whereas only minor changes were observed in total RNA preparations (Figure S1A). This result was expected since total RNA predominantly contains other m^6A-modified RNAs, which are not methylated by METTL3. Interestingly, when we performed a time course experiment in which we monitored global m^6A mRNA methylation for one week, m^6A methylation levels did not decrease further, but remained at the initial reduced level (Figure 2B). To assess the potential impact of rRNA contaminations, we also analyzed m_2^6A levels in our samples (Figures S1B–S1D) and observed no significant differences between control (scramble) and knockout preparations. These results confirmed the depletion of rRNA during mRNA purification and exclude a major contribution of contaminating rRNA to the measured m^6A levels.

The retention of reduced m^6A methylation levels raised the possibility of positive selection for cells that express catalytically active METTL3.[16] We therefore isolated single clones from our knockout cell populations and cultivated them for several weeks. Western blot analyses detected the wild-type protein in several of the clones derived from both cell lines (Figure 2C). Furthermore, T24 clone S showed an additional METTL3 immunoreactive band of lower molecular weight (Figure 2C), indicating that this clone expresses a CRISPR/Cas9-induced isoform of METTL3. This band was detectable in almost all UM-UC-3 clones (Figure 2C), but not when the cell pool was harvested only 24 h after knockout induction (Figure 1A). Consistent with a recently published report,[16] these findings suggest that METTL3 is required for T24 and UM-UC-3 cell viability.

To further investigate the requirements for METTL3 in UCB cell lines, we analyzed the degree of METTL3 dependency in the 30 UCB cell lines included in the DepMap database, which quantifies cell viability after systematic protein depletion in CRISPR/Cas9-mediated screens.[19] The analysis showed dependency probability scores >0.5 for the majority of UCB cell lines (Figure 2D), including T24 and UM-UC-3. We then

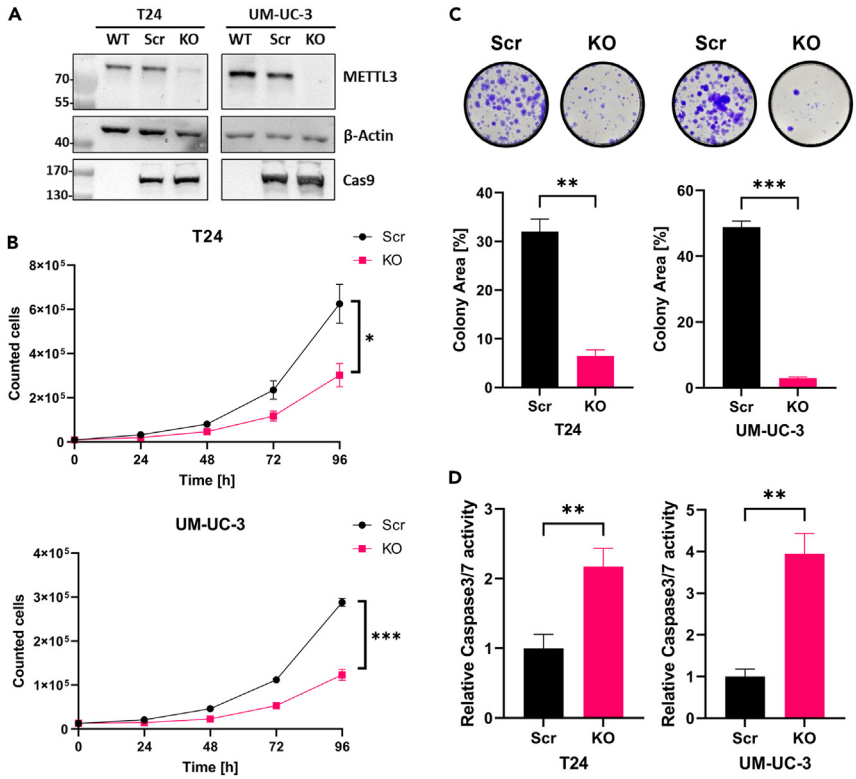

Figure 1. METTL3 depletion reduces the oncogenic phenotype of UCB cell lines

(A) Immunoblot demonstrating the loss of METTL3 in T24 and UM-UC-3 cell lines 24 h after CRISPR/Cas9-induced *METTL3* knockout. WT = wild-type, Scr = scramble, KO = knockout.

(B) In cell counting assays, *METTL3* knockout cells were characterized by reduced cell growth. *$p < 0.05$, ***$p < 0.001$, two-way analysis of variance.

(C) *METTL3* knockout cells showed impaired clonogenicity in colony formation assays. **$p < 0.01$, ***$p < 0.001$, two-tailed Student's *t* test.

(D) Enhanced Caspase 3/7 activity in *METTL3* knockout cells indicated a significant upregulation of apoptosis signaling determined by Caspase Glo assays. **$p < 0.01$, two-tailed Student's *t* test. Data are represented as mean ± SD.

broadened our analysis to include all other cell lines (n = 1056) from the DepMap database and obtained a similar result (Figure S2A). Further comparisons to presumed essential (*POLR2F*) and non-essential (*DNMT2*/*TRDMT1*) control genes revealed dependency probability scores that were consistently high and low, respectively (Figure S2A). These findings further illustrate that METTL3 expression is required for survival.

We also investigated the expression level of METTL3 protein in a panel of uroepithelial and UCB cell lines. UROtsa uroepithelial, RT112/84 and T24 UCB cells showed similar expression levels, while RT4 and UM-UC-3 UCB cells showed higher METTL3 expression (Figure S2B). When these cells were treated with the METTL3 inhibitor STM2457,[10] they showed a robust concentration-dependent decrease in cell viability, with no major differences between uroepithelial and UCB cells (Figure 2E). To investigate whether these antiproliferative effects were caused by a specific inhibition of the METTL3 methyltransferase activity, we analyzed STM2457-treated T24 and UM-UC-3 cells in LC-MS/MS and Western blot experiments. LC-MS/MS results revealed a relative decrease in global m^6A mRNA levels of approximately 75% (Figure S2C), while there were no major differences in rRNA contamination levels (Figure S1E). METTL3 protein levels were unaffected by the inhibitor treatment in UM-UC-3 cells and slightly increased in T24 cells (Figure S2D), suggesting that the effect of METTL3 on cell viability is indeed caused by the inhibition of the methyltransferase activity and not by other METTL3-mediated functions. Taken together, these findings indicate that UCB and uroepithelial cells depend on the METTL3 activity for cell viability and suggest a narrow therapeutic window for METTL3-inhibiting drugs in UCB.

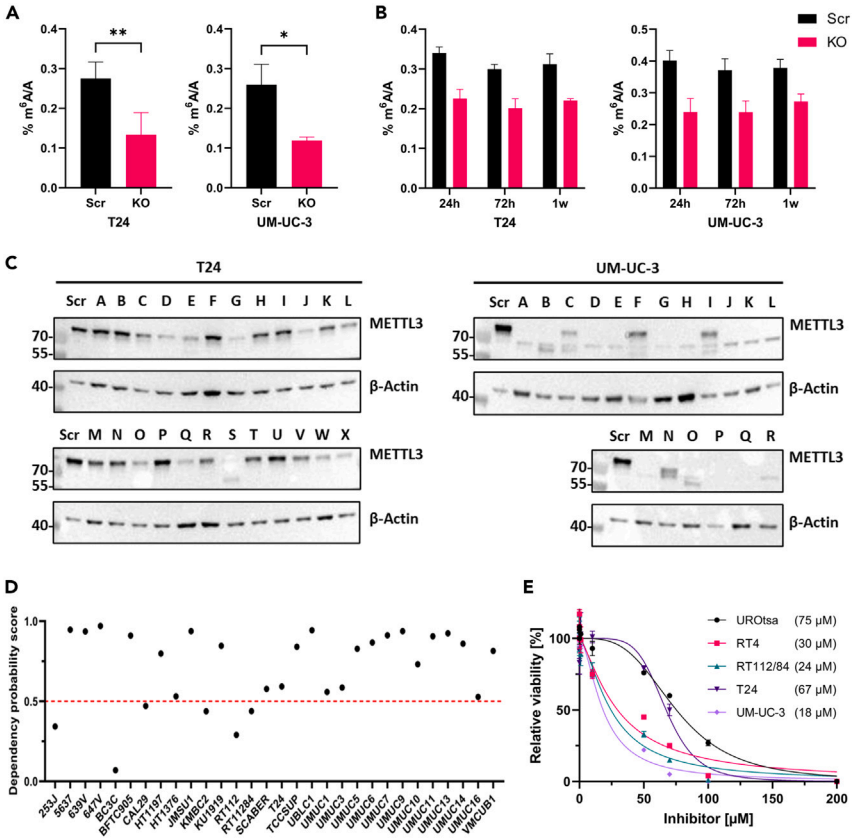

Figure 2. METTL3 activity is essential for viability in uroepithelial and UCB cells

(A) *METTL3* knockout decreased the global m^{6}A mRNA methylation levels 24 h after knockout induction. In T24 knockout cells, a relative reduction of 51% was observed. In UM-UC-3 knockout cells, a relative reduction of 54% was observed. *$p < 0.05$, **$p < 0.01$, two-tailed Student's *t* test.

(B) Monitoring of m^{6}A mRNA levels over one week after knockout induction revealed that they did not decrease further but remained constant. Technical triplicates were analyzed from two biological replicates.

(C) The screening of *METTL3* knockout cell clones revealed the presence of heterozygous cells and cells expressing potential CRISPR/Cas9-induced isoforms of METTL3.

(D) DepMap data analysis of METTL3 dependencies in a panel of UCB cell lines. Dependency probability scores demonstrated that the majority of UCB cell lines most likely depends on METTL3 expression for viability. Concerning dependency probability scores, a cell line is considered dependent if it has a probability of dependency greater than 0.5.

(E) STM2457 inhibitor response curves for represented cell lines indicate that the uroepithelial UROtsa cell line also depends on METTL3 for viability. IC_{50} values for each cell line are shown in brackets. See also Figures S1 and S2. Data are represented as mean ± SD.

METTL3 knockout clones maintain a level of m^{6}A modification required for UCB cell viability

In further experiments, we also used LC-MS/MS and cellular assays to assess the impact of the detected METTL3 isoforms on global m^{6}A mRNA methylation, cell proliferation, clonogenicity, and apoptosis. LC-MS/MS analyses revealed a relative reduction of global m^{6}A mRNA levels between 41 and 47% in T24 clones, while global m^{6}A mRNA levels of UM-UC-3 clones were decreased by 63 and 71%, respectively, indicating that the detected METTL3 isoforms have catalytic activity ($p < 0.0001$, one-way analysis of variance, Figure 3A). We found significantly more rRNA contaminants in T24 control cells compared to T24 clones Q and S suggesting that the LC-MS/MS measurements even overestimated the difference in m^{6}A mRNA methylation levels ($p < 0.01$, one-way analysis of variance, Figure S1F). Regarding cell proliferation, no significant changes were observed between control cells and *METTL3* knockout clones in the T24 cell line, while UM-UC-3 *METTL3* knockout clones showed a significant decrease in proliferation ($p < 0.0001$, two-way analyses of variance, Figure 3B). In both cell lines, *METTL3* knockout clones were characterized by reduced colony formation (T24 clones J and Q: $p < 0.01$, clone S: $p < 0.0001$; UM-UC-3: $p < 0.0001$, one-way analysis of variance, Figure 3C) and increased Caspase 3/7 activity (T24 clone J: $p < 0.01$, clone

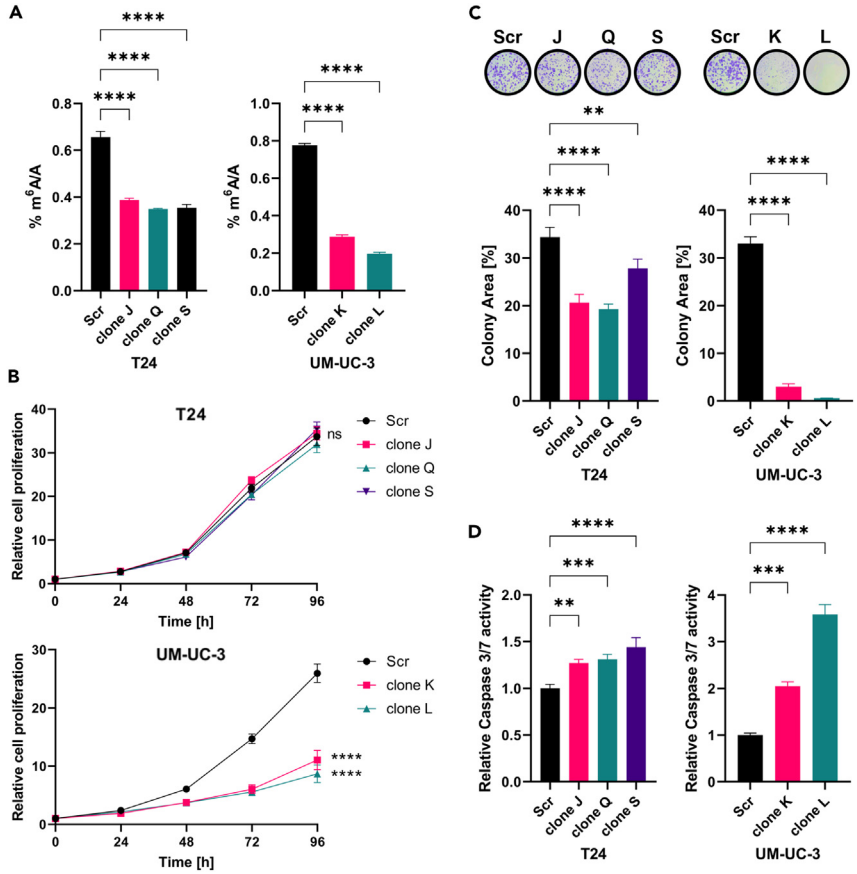

Figure 3. *METTL3* knockout clones maintain reduced levels of m^{6}A modification required for UCB cell viability

(A) LC-MS/MS measurements of *METTL3* knockout clones showed a decrease in global m^{6}A mRNA levels. In T24 knockout clones, a relative reduction of 41–47% was observed. In UM-UC-3 knockout clones, a relative reduction of 63 resp. 71% was observed. ****p < 0.0001, one-way analysis of variance.

(B) In cell proliferation assays, no significant changes between T24 Scr and *METTL3* knockout clones were observed. ns = not significant, two-way analysis of variance. UM-UC-3 *METTL3* knockout clones showed a significant decrease in cell growth. ****p < 0.0001, two-way analysis of variance.

(C) *METTL3* knockout clones showed impaired clonogenicity. **p < 0.01, ****p < 0.0001, one-way analysis of variance.

(D) In Caspase activity assays, *METTL3* knockout clones showed increased apoptosis signaling. **p < 0.01, ***p < 0.001, ****p < 0.0001, one-way analysis of variance. See also Figure S1. Data are represented as mean ± SD.

Q: p < 0.001, clone S: p < 0.0001; UM-UC-3 clone K: p < 0.001, clone L: p < 0.0001, one-way analysis of variance, Figure 3D). All viable heterozygous clones and clones expressing aberrant isoforms of METTL3 retained a minimum level of approximately 0.2% m^{6}A/A, suggesting that this level is required for UCB cell viability.

Elevated *METTL3* expression levels in UCB are not associated with poor UCB prognosis and do not cause a global increase in m^{6}A levels

To investigate the clinical relevance of our cell-based results, we analyzed *METTL3* mRNA expression and METTL3-dependent survival in two independent cohorts of UCB patients (TCGA cohort, n = 425 and UKMA validation cohort, n = 102). The clinicopathological details of both cohorts are summarized in Table S1. *METTL3* expression analysis revealed significantly elevated mRNA expression levels in TCGA UCB samples compared to para-tumoral tissue (p < 0.0001, Mann-Whitney-U test, Figure 4A). We also detected significantly higher *METTL3* expression in grade 3 tumors relative to grade 2 carcinomas in the UKMA validation cohort (p < 0.05, Mann-Whitney-U test, Figure 4B). However, neither cohort showed significant differences in *METTL3* expression across the different T-stages (TCGA cohort: p = 0.1189, UKMA validation cohort: p = 0.9862, chi-square-test, Figure 4C). We then examined METTL3 protein expression by

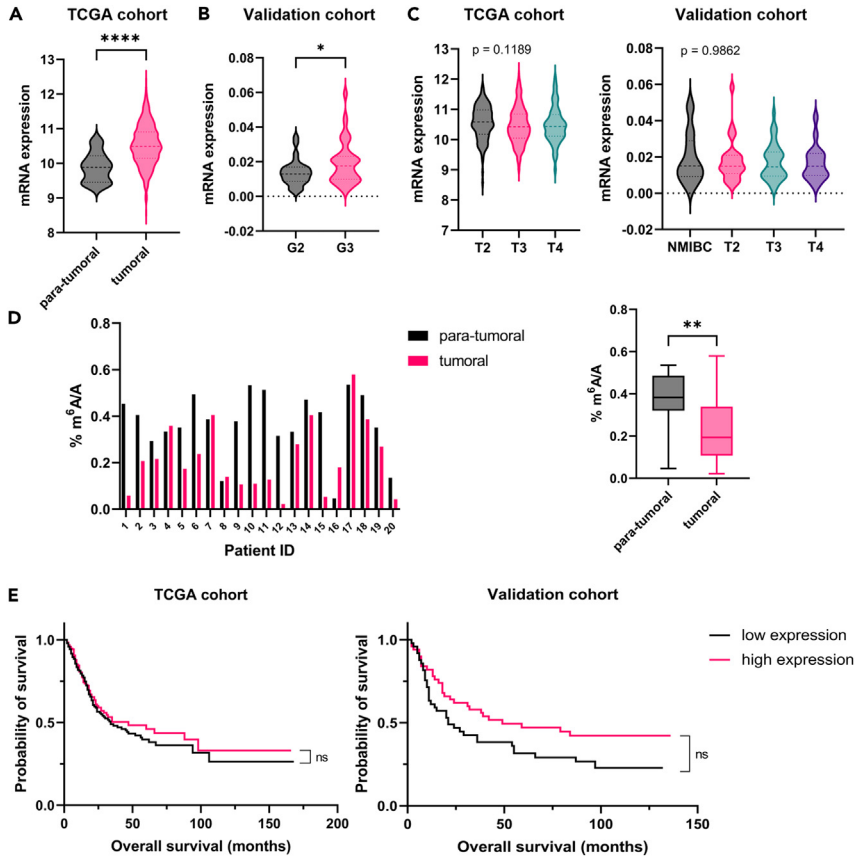

Figure 4. Elevated *METTL3* expression levels in UCB are not associated with poor UCB prognosis and do not cause a global increase in m^{6}A levels

(A) Elevated *METTL3* mRNA expression levels in UCB compared to para-tumoral tissue. ****p < 0.0001, Mann-Whitney-U test.

(B) Elevated *METTL3* mRNA expression levels in poorly differentiated tumors (grade 3) compared to more differentiated (grade 2) tumors. *p < 0.05, Mann-Whitney-U test.

(C) Stable levels of METTL3 mRNA expression across all tumor stages and in both cohorts. TCGA p = 0.1189, UKMA p = 0.9862, chi-square-test.

(D) LC-MS/MS analyses revealed significantly higher m^{6}A mRNA methylation levels in para-tumoral tissue samples compared to UCB tissue samples. **p < 0.01, Mann-Whitney-U test.

(E) Kaplan-Meier plots showing overall survival of UCB patients stratified according to *METTL3* expression. ns = not significant (TCGA p = 0.4630, UKMA p = 0.0594), log rank test. Black lines indicate low expression, pink lines indicate high expression. See also Figures S3 and S4 and Tables S1–S3. The violin plots represent the median and quartiles. The boxplot represents the median and the interquartile range of values. Whiskers extend to the minimum and maximum values.

immunohistochemistry in UCB tissue samples comprising Ta, Tis, and T2 stages (n = 5 for each stage, Figure S3A, Table S2). In accordance with mRNA expression analyses, METTL3 protein expression levels were found to be significantly increased in tumoral tissues compared to para-tumoral tissue (p < 0.01, Mann-Whitney-U test, Figure S3B), as reported previously.[13] However, they did not change significantly among the different tumor stages (p > 0.99, chi-square-test, Figure S3B), which is again consistent with published results.[14]

To investigate whether the increased expression of METTL3 in UCB is accompanied with globally elevated m^{6}A levels, we isolated mRNA from 20 pairs of UCB tumor and para-tumoral tissue samples, respectively, and analyzed their global m^{6}A mRNA methylation levels via LC-MS/MS (Table S3). Interestingly, m^{6}A mRNA methylation levels were found to be significantly lower in tumors compared to para-tumoral tissue (p < 0.01, Mann-Whitney-U test, Figure 4D), while no significant difference in m_2^6A levels was detected in

quality controls (Figure S3C). To provide a possible explanation for the apparent discrepancy between reduced m^{6}A mRNA methylation levels and increased METTL3 expression, we analyzed the expression levels of all m^{6}A writer complex components in the TCGA dataset. While METTL3 was upregulated (Figures 4A and S4), METTL14, WTAP, and ZC3H13 were found to be downregulated in UCB patients (WTAP: $p < 0.01$, METTL14 and ZC3H13: $p < 0.0001$, Mann-Whitney-U test, Figure S4) indicating a potential stochiometric imbalance of m^{6}A writer complex subunits that could result in reduced m^{6}A mRNA methylation levels in UCB samples.

Finally, we also performed survival time analyses to re-examine the clinical role of METTL3 in UCB. Interestingly, the results showed that higher levels of METTL3 expression were not associated with poor patient prognosis in both cohorts (TCGA cohort: $p = 0.46$, log rank test; UKMA validation cohort: $p = 0.059$, log rank test, Figure 4E). These findings are contrary to published survival data from 180 bladder cancer patients[14] and also unexpected in light of the reduced oncogenic phenotypes observed in METTL3-deficient UCB cells. Taken together, our findings suggest that METTL3 overexpression is not linked to UCB progression, and that the role of the enzyme in this tumor type is more complex than the cell-based results suggest.

DISCUSSION

In this study, we challenge the widespread notion that METTL3 acts as a classical oncogene in UCB[12] and critically examine the value of METTL3 as a useful diagnostic and prognostic biomarker in UCB.[14] METTL3 is the most important m^{6}A-catalyzing enzyme and responsible for >95% of m^{6}A in mRNA.[20] It was also shown that *METTL3* knockout cells often express active METTL3 isoforms to maintain the m^{6}A levels required for cell survival.[16] Considering these findings, we re-examined METTL3 dependency and function in UCB and critically analyzed its clinical relevance for UCB patients.

METTL3 and its role in the m^{6}A network is crucial for a functional RNA metabolism. Thus, the dysregulation of METTL3 is implicated in several cancer entities.[9] However, METTL3 has been associated with vastly different roles in oncogenesis across different tumor entities. For example, while METTL3 acts as a tumor suppressor in endometrial cancer[21] and thyroid cancer,[22] it shows oncogenic activities in colon[23] and lung cancer.[24] In UCB, the role of METTL3 is discussed controversially. Several studies declare METTL3 to be an oncogene in UCB,[13,14,17,25–27] while the enzyme was also found to be a potential tumor suppressor.[15] The decreased proliferation rate, impaired clonogenicity and increased apoptosis observed in our METTL3-deficient T24 and UM-UC-3 cells are consistent with the reported oncogenic effects of METTL3 in UCB.

In our *METTL3* knockout approach, we aimed to prevent the formation of functional METTL3 isoforms by using an inducible CRISPR/Cas9 system with four different sgRNAs.[28] Interestingly, despite our complex knockout approach, we identified heterozygous clones expressing the METTL3 wild-type protein and clones expressing CRISPR/Cas9-induced METTL3 isoforms in both cell lines. Also, we performed LC-MS/MS-based m^{6}A quantification of our METTL3-deficient cell lines and detected a global decrease, but not to a complete loss of m^{6}A mRNA methylation. Time-dependent monitoring of global m^{6}A mRNA methylation after *METTL3* knockout showed that m^{6}A methylation levels did not decrease further over time but remained at the initially observed, reduced level. These findings suggest that partial METTL3 activity is maintained by heterozygous cells and cells expressing catalytically active isoforms to preserve the baseline levels of m^{6}A that are required for survival.[16] The results obtained with several heterozygous *METTL3* knockout clones and clones expressing aberrant isoforms of METTL3 supported these observations and indicated that METTL3 isoforms have remaining catalytic activity. Furthermore, our results suggest that data obtained with other *METTL3* UCB knockout cell lines reported in the literature[17,27] should be interpreted with caution. DepMap analysis additionally confirmed that METTL3 activity is critical for cell viability in most UCB cell lines, but also in cell lines from all other cancer entities. STM2457 inhibitor response curves supported these findings and extended them to uroepithelial cells. Interestingly, the observed IC_{50} values for the tested UCB cell lines (18–75 μM) were considerably higher than the published[10] IC_{50} values for AML cell lines (0.6–10.3 μM), indicating differential sensitivities among cancer entities.

Concerning our clinical data analyses, the higher *METTL3* expression in UCB compared to para-tumoral tissue and in more aggressive UCB contrasts with the observation that no difference in METTL3 expression could be found between non-muscle-invasive UCB and muscle-invasive UCB. In addition, high METTL3 expression in UCB samples was not associated with poor prognosis in both cohorts, which is contradictory to a previous study.[14] However, this study used METTL3 expression results obtained from immunohistochemistry analysis,

which are often less specific and more difficult to quantify. Furthermore, our LC-MS/MS results revealed significantly lower m^{6}A mRNA levels in UCB tissues compared to the corresponding para-tumoral tissues. As such, METTL3 upregulation in UCB does not lead to increased global m^{6}A mRNA methylation levels. These findings represent a considerable expansion of published LC-MS/MS data, which suggested a 2- to 3-fold increase in m^{6}A mRNA methylation levels for UCB.[13] However, this analysis was based on only two tumor samples and lacked controls for the detection of rRNA contamination. Notably, we found several m^{6}A writer complex components to be significantly downregulated in UCB patients. This observation raises the possibility that the observed downregulation of global m^{6}A mRNA levels is caused by a stochiometric imbalance or dysregulation[29,30] of the m^{6}A writer complex subunits that potentially disturbs the formation of functionally active writer complexes.

The observation that METTL3 expression did not differ across tumor stages may be explained by the fact that these stages are more reflective of the timing of UCB diagnosis and surgical therapy. This timing is crucial in UCB management and has the biggest impact on the prognosis because it correlates with the likelihood of metastatic disease in more advanced stages. Our findings also suggest that METTL3 may not be a suitable target for local or systemic treatment of UCB, as m^{6}A mRNA methylation is required for the survival of both healthy and malignant cells. This notion is supported by our inhibitor response and LC-MS/MS analyses, as well as by the reported *METTL3* knockout mouse phenotype, which is characterized by early embryonic lethality.[7] As a consequence, the therapeutic window of METTL3 inhibiting drugs may be very narrow for UCB patients, resulting in clinical side effects that mask the therapeutic benefit. Additionally, METTL3 inhibition may lead to a rapid treatment escape and failure by the expression of cryptic, catalytically active METTL3 isoforms.[16] Thus, the clinical potential of METTL3 in UCB might rather lie in biomarker development for survival prognosis or response to therapy – either alone or in combination with other m^{6}A-associated factors.

Limitations of the study

Further research should be carried out to better characterize the alternative METTL3 isoforms in our knockout cell lines, for example by 5′ RACE (rapid amplification of cDNA ends). This could confirm whether these isoforms still encode the methyltransferase domain or domains required for assembly with further components of the methyltransferase complex, like METTL14 or WTAP. Concerning clinical data analyses, further work should explore the relationship between increased METTL3 expression and reduced m^{6}A mRNA methylation levels in UCB samples. We also assume that the global methylation loss will affect locus-specific methylation patterns. Transcriptome-wide mapping at base-resolution and stochiometric quantification of m^{6}A, like in the recently established GLORI protocol,[31] should be pursued to gain further insights into these changes. Finally, although METTL3 is consistently upregulated in UCB among different cohorts, its effect on UCB patient survival remains controversial. To resolve this contradiction, analyses of more and larger cohorts are needed.

STAR★METHODS

Detailed methods are provided in the online version of this paper and include the following:

- KEY RESOURCES TABLE
- RESOURCE AVAILABILITY
  - Lead contact
  - Materials availability
  - Data and code availability
- EXPERIMENTAL MODEL AND STUDY PARTICIPANT DETAILS
  - Patients and patient samples
  - Cell culture
- METHOD DETAILS
  - Establishment of conditional *METTL3* knockout cell lines
  - Cell proliferation, clonogenicity and apoptosis assays
  - Inhibitor response assay
  - Western blotting
  - Immunohistochemistry
  - Liquid chromatography-tandem mass spectrometry (LC-MS/MS) for the analysis of m^{6}A mRNA methylation levels

- Quantitative real-time PCR for METTL3 expression analysis
- In-silico data analysis
- DepMap analysis
- QUANTIFICATION AND STATISTICAL ANALYSIS

SUPPLEMENTAL INFORMATION

Supplemental information can be found online at https://doi.org/10.1016/j.isci.2023.107300.

ACKNOWLEDGMENTS

M.Ne. acknowledges funding by the Deutsche Gesellschaft für Urologie (DGU, German Society of Urology) – Ferdinand Eisenberger research fellowship (grant number NeM1/FE-20). M.Ni. acknowledges funding by Viktor & Sigrid Dulger Stiftung – research fellowship ProMinent. F.L. acknowledges funding by Deutsche Forschungsgemeinschaft (DFG, German Research Foundation) – project number 439669440 TRR319 RMaP TP A01. M.H. acknowledges funding by Deutsche Forschungsgemeinschaft (DFG, German Research Foundation) – project number 439669440 TRR319 RMaP TP C03. Support by the DKFZ Light Microscopy Facility is gratefully acknowledged. We also thank Tanja Musch for help with cell culture.

AUTHOR CONTRIBUTIONS

J.K., M.Ne., M.Ni., and F.L.: Conceptualization. J.K., M.Ne., M.S-D., J.X., and M.Ni.: Investigation, Formal Analysis, and Visualization. M.H., J.E., M.C.K., P.N., P.E., M.S.M., and F.L.: Resources. V.C.C., M.R-P., and F.L.: Supervision. J.K., M.Ne., M.Ni., and F.L.: Writing – Original Draft. All authors: Writing – Review and Editing.

DECLARATION OF INTERESTS

M.H. is a consultant for Moderna Inc.

Received: March 2, 2023
Revised: June 13, 2023
Accepted: July 3, 2023
Published: July 11, 2023

REFERENCES

1. Siegel, R.L., Miller, K.D., Wagle, N.S., and Jemal, A. (2023). Cancer statistics, 2023. CA. CA A Cancer J. Clin. *73*, 17–48. https://doi.org/10.3322/caac.21763.

2. Berdik, C. (2017). Unlocking bladder cancer. Nature *551*, 34–35. https://doi.org/10.1038/551S34a.

3. Zaccara, S., Ries, R.J., and Jaffrey, S.R. (2019). Reading, writing and erasing mRNA methylation. Nat. Rev. Mol. Cell Biol. *20*, 608–624. https://doi.org/10.1038/s41580-019-0168-5.

4. Wang, X., Feng, J., Xue, Y., Guan, Z., Zhang, D., Liu, Z., Gong, Z., Wang, Q., Huang, J., Tang, C., et al. (2016). Structural basis of N(6)-adenosine methylation by the METTL3-METTL14 complex. Nature *534*, 575–578. https://doi.org/10.1038/nature18298.

5. Jiang, X., Liu, B., Nie, Z., Duan, L., Xiong, Q., Jin, Z., Yang, C., and Chen, Y. (2021). The role of m6A modification in the biological functions and diseases. Signal Transduct. Targeted Ther. *6*, 74. https://doi.org/10.1038/s41392-020-00450-x.

6. Batista, P.J., Molinie, B., Wang, J., Qu, K., Zhang, J., Li, L., Bouley, D.M., Lujan, E., Haddad, B., Daneshvar, K., et al. (2014). m6A RNA Modification Controls Cell Fate Transition in Mammalian Embryonic Stem Cells. Cell Stem Cell *15*, 707–719. https://doi.org/10.1016/j.stem.2014.09.019.

7. Geula, S., Moshitch-Moshkovitz, S., Dominissini, D., Mansour, A.A., Kol, N., Salmon-Divon, M., Hershkovitz, V., Peer, E., Mor, N., Manor, Y.S., et al. (2015). Stem cells. m6A mRNA methylation facilitates resolution of naïve pluripotency toward differentiation. Science *347*, 1002–1006. https://doi.org/10.1126/science.1261417.

8. Lan, Q., Liu, P.Y., Haase, J., Bell, J.L., Hüttelmaier, S., and Liu, T. (2019). The Critical Role of RNA m(6)A Methylation in Cancer. Cancer Res. *79*, 1285–1292. https://doi.org/10.1158/0008-5472.Can-18-2965.

9. He, L., Li, H., Wu, A., Peng, Y., Shu, G., and Yin, G. (2019). Functions of N6-methyladenosine and its role in cancer. Mol. Cancer *18*, 176. https://doi.org/10.1186/s12943-019-1109-9.

10. Yankova, E., Blackaby, W., Albertella, M., Rak, J., De Braekeleer, E., Tsagkogeorga, G., Pilka, E.S., Aspris, D., Leggate, D., Hendrick, A.G., et al. (2021). Small-molecule inhibition of METTL3 as a strategy against myeloid leukaemia. Nature *593*, 597–601. https://doi.org/10.1038/s41586-021-03536-w.

11. Chen, M., Nie, Z.-y., Wen, X.-h., Gao, Y.-h., Cao, H., and Zhang, S.-f. (2019). m6A RNA methylation regulators can contribute to malignant progression and impact the prognosis of bladder cancer. Biosci. Rep. *39*. https://doi.org/10.1042/bsr20192892.

12. Liu, Q. (2021). Current Advances in N6-Methyladenosine Methylation Modification During Bladder Cancer. Front. Genet. *12*, 825109. https://doi.org/10.3389/fgene.2021.825109.

13. Cheng, M., Sheng, L., Gao, Q., Xiong, Q., Zhang, H., Wu, M., Liang, Y., Zhu, F., Zhang, Y., Zhang, X., et al. (2019). The m(6)A methyltransferase METTL3 promotes bladder cancer progression via AFF4/NF-κB/MYC signaling network. Oncogene *38*, 3667–3680. https://doi.org/10.1038/s41388-019-0683-z.

14. Han, J., Wang, J.Z., Yang, X., Yu, H., Zhou, R., Lu, H.C., Yuan, W.B., Lu, J.C., Zhou, Z.J., Lu, Q., et al. (2019). METTL3 promote tumor proliferation of bladder cancer by accelerating pri-miR221/222 maturation in

m6A-dependent manner. Mol. Cancer *18*, 110. https://doi.org/10.1186/s12943-019-1036-9.

15. Zhao, S., Liu, J., Nanga, P., Liu, Y., Cicek, A.E., Knoblauch, N., He, C., Stephens, M., and He, X. (2019). Detailed modeling of positive selection improves detection of cancer driver genes. Nat. Commun. *10*, 3399. https://doi.org/10.1038/s41467-019-11284-9.

16. Poh, H.X., Mirza, A.H., Pickering, B.F., and Jaffrey, S.R. (2022). Alternative splicing of METTL3 explains apparently METTL3-independent m6A modifications in mRNA. PLoS Biol. *20*, e3001683. https://doi.org/10.1371/journal.pbio.3001683.

17. Jin, H., Ying, X., Que, B., Wang, X., Chao, Y., Zhang, H., Yuan, Z., Qi, D., Lin, S., Min, W., et al. (2019). N6-methyladenosine modification of ITGA6 mRNA promotes the development and progression of bladder cancer. EBioMedicine *47*, 195–207. https://doi.org/10.1016/j.ebiom.2019.07.068.

18. Xie, H., Li, J., Ying, Y., Yan, H., Jin, K., Ma, X., He, L., Xu, X., Liu, B., Wang, X., et al. (2020). METTL3/YTHDF2 m(6) A axis promotes tumorigenesis by degrading SETD7 and KLF4 mRNAs in bladder cancer. J. Cell Mol. Med. *24*, 4092–4104. https://doi.org/10.1111/jcmm.15063.

19. Dempster, J.M., Boyle, I., Vazquez, F., Root, D.E., Boehm, J.S., Hahn, W.C., Tsherniak, A., and McFarland, J.M. (2021). Chronos: a cell population dynamics model of CRISPR experiments that improves inference of gene fitness effects. Genome Biol. *22*, 343. https://doi.org/10.1186/s13059-021-02540-7.

20. Murakami, S., and Jaffrey, S.R. (2022). Hidden codes in mRNA: Control of gene expression by m(6)A. Mol. Cell. *82*, 2236–2251. https://doi.org/10.1016/j.molcel.2022.05.029.

21. Liu, J., Eckert, M.A., Harada, B.T., Liu, S.M., Lu, Z., Yu, K., Tienda, S.M., Chryplewicz, A., Zhu, A.C., Yang, Y., et al. (2018). m(6)A mRNA methylation regulates AKT activity to promote the proliferation and tumorigenicity of endometrial cancer. Nat. Cell Biol. *20*, 1074–1083. https://doi.org/10.1038/s41556-018-0174-4.

22. He, J., Zhou, M., Yin, J., Wan, J., Chu, J., Jia, J., Sheng, J., Wang, C., Yin, H., and He, F. (2021). METTL3 restrains papillary thyroid cancer progression via m(6)A/c-Rel/IL-8-mediated neutrophil infiltration. Mol. Ther. *29*, 1821–1837. https://doi.org/10.1016/j.ymthe.2021.01.019.

23. Li, T., Hu, P.S., Zuo, Z., Lin, J.F., Li, X., Wu, Q.N., Chen, Z.H., Zeng, Z.L., Wang, F., Zheng, J., et al. (2019). METTL3 facilitates tumor progression via an m(6)A-IGF2BP2-dependent mechanism in colorectal carcinoma. Mol. Cancer *18*, 112. https://doi.org/10.1186/s12943-019-1038-7.

24. Choe, J., Lin, S., Zhang, W., Liu, Q., Wang, L., Ramirez-Moya, J., Du, P., Kim, W., Tang, S., Sliz, P., et al. (2018). mRNA circularization by METTL3-eIF3h enhances translation and promotes oncogenesis. Nature *561*, 556–560. https://doi.org/10.1038/s41586-018-0538-8.

25. Ni, Z., Sun, P., Zheng, J., Wu, M., Yang, C., Cheng, M., Yin, M., Cui, C., Wang, G., Yuan, L., et al. (2022). JNK Signaling Promotes Bladder Cancer Immune Escape by Regulating METTL3-Mediated m6A Modification of PD-L1 mRNA. Cancer Res. *82*, 1789–1802. https://doi.org/10.1158/0008-5472.Can-21-1323.

26. Wang, G., Dai, Y., Li, K., Cheng, M., Xiong, G., Wang, X., Chen, S., Chen, Z., Chen, J., Xu, X., et al. (2021). Deficiency of Mettl3 in Bladder Cancer Stem Cells Inhibits Bladder Cancer Progression and Angiogenesis. Front. Cell Dev. Biol. *9*, 627706. https://doi.org/10.3389/fcell.2021.627706.

27. Yang, F., Jin, H., Que, B., Chao, Y., Zhang, H., Ying, X., Zhou, Z., Yuan, Z., Su, J., Wu, B., et al. (2019). Dynamic m(6)A mRNA methylation reveals the role of METTL3-m(6)A-CDCP1 signaling axis in chemical carcinogenesis. Oncogene *38*, 4755–4772. https://doi.org/10.1038/s41388-019-0755-0.

28. Mou, H., Smith, J.L., Peng, L., Yin, H., Moore, J., Zhang, X.O., Song, C.Q., Sheel, A., Wu, Q., Ozata, D.M., et al. (2017). CRISPR/Cas9-mediated genome editing induces exon skipping by alternative splicing or exon deletion. Genome Biol. *18*, 108. https://doi.org/10.1186/s13059-017-1237-8.

29. Zheng, B., Wang, J., Zhao, G., Chen, X., Yao, Z., Niu, Z., and He, W. (2021). A new m6A methylation-related gene signature for prognostic value in patient with urothelial carcinoma of the bladder. Biosci. Rep. *41*, BSR20204456. https://doi.org/10.1042/BSR20204456.

30. Guimarães-Teixeira, C., Lobo, J., Miranda-Gonçalves, V., Barros-Silva, D., Martins-Lima, C., Monteiro-Reis, S., Sequeira, J.P., Carneiro, I., Correia, M.P., Henrique, R., and Jerónimo, C. (2022). Downregulation of m6A writer complex member METTL14 in bladder urothelial carcinoma suppresses tumor aggressiveness. Mol. Oncol. *16*, 1841–1856. https://doi.org/10.1002/1878-0261.13181.

31. Liu, C., Sun, H., Yi, Y., Shen, W., Li, K., Xiao, Y., Li, F., Li, Y., Hou, Y., Lu, B., et al. (2023). Absolute quantification of single-base m6A methylation in the mammalian transcriptome using GLORI. Nat. Biotechnol. *41*, 355–366. https://doi.org/10.1038/s41587-022-01487-9.

32. Barger, C.J., Branick, C., Chee, L., and Karpf, A.R. (2019). Pan-Cancer Analyses Reveal Genomic Features of FOXM1 Overexpression in Cancer. Cancers *11*, 251. https://doi.org/10.3390/cancers11020251.

33. Schneider, C.A., Rasband, W.S., and Eliceiri, K.W. (2012). NIH Image to ImageJ: 25 years of image analysis. Nat. Methods *9*, 671–675. https://doi.org/10.1038/nmeth.2089.

34. Guzmán, C., Bagga, M., Kaur, A., Westermarck, J., and Abankwa, D. (2014). ColonyArea: an ImageJ plugin to automatically quantify colony formation in clonogenic assays. PLoS One *9*, e92444. https://doi.org/10.1371/journal.pone.0092444.

35. Fedchenko, N., and Reifenrath, J. (2014). Different approaches for interpretation and reporting of immunohistochemistry analysis results in the bone tissue - a review. Diagn. Pathol. *9*, 221. https://doi.org/10.1186/s13000-014-0221-9.

36. Thüring, K., Schmid, K., Keller, P., and Helm, M. (2016). Analysis of RNA modifications by liquid chromatography-tandem mass spectrometry. Methods *107*, 48–56. https://doi.org/10.1016/j.ymeth.2016.03.019.

STAR★METHODS

KEY RESOURCES TABLE

REAGENT or RESOURCE	SOURCE	IDENTIFIER
Antibodies		
METTL3 antibody (for Western blot)	Proteintech	Cat#15073-1-AP; RRID: AB_2142033
METTL3 antibody (for IHC)	Abcam	Cat#ab195352; RRID: AB_2721254
β-Actin antibody	Santa Cruz Biotechnology	Cat#sc-47778; RRID: AB_626632
Cas9 antibody	Epigentek	Cat#A-9000; RRID: AB_2828022
Biological samples		
UCB patient samples for the analysis of *METTL3* expression via quantitative real-time PCR (UKMA cohort, Table S1)	Department of Urology and Urosurgery at the University Hospital of Mannheim	N/A
UCB patient tissue sections for the analysis of METTL3 expression via IHC (Table S2)	Department of Urology and Urosurgery at the University Hospital of Mannheim	N/A
UCB patient samples for the analysis of m^6A mRNA levels via LC-MS/MS (Table S3)	Department of Urology and Urosurgery at the University Hospital of Mannheim	N/A
Chemicals, peptides, and recombinant proteins		
METTL3 inhibitor STM2457	MedChemExpress	Cat#HY-134836
Mesa Green qPCR MasterMix Plus for SYBR	Eurogentec	Cat#RT-SY2X-03+WOU
Nuclease P1 from *Penicillium citrinum*	Sigma-Aldrich	Cat#N8630
Snake venom phosphodiesterase from *C. adamanteus*	Worthington	Cat#LS003926
Bovine intestine phosphatase	Sigma-Aldrich	Cat#P0114
Benzonase	Sigma-Aldrich	Cat#E1014
Pentostatin	Sigma-Aldrich	Cat#SML0508
Tetrahydrouridine	Merck Millipore	Cat#584222
Critical commercial assays		
Cell Titer-Glo Luminescent Cell Viability Assay kit	Promega	Cat#G7571
Caspase-Glo 3/7 Assay kit	Promega	Cat#G8091
Dynabeads mRNA purification kit	Thermo Fisher Scientific	Cat#61006
XTRAKT FFPE kit	Stratifyer	Cat#XTK2.0-96
SuperScript III First-Strand Synthesis System	Thermo Fisher Scientific	Cat#18080-044
Deposited data		
22Q2 CRISPR gene dependency dataset	Depmap https://depmap.org/portal/download/all/	22Q2
TCGA RNA-Seq data (HiSeq) of the bladder urothelial carcinoma dataset	TCGA	Project-ID: TCGA-BLCA
Experimental models: Cell lines		
UROtsa	European Collection of Authenticated Cell Cultures (ECACC)	RRID: CVCL_0571
HEK293T	ECACC	RRID: CVCL_0063
RT112/84	ECACC	RRID: CVCL_2714
UM-UC-3	ECACC	RRID: CVCL_1783

(*Continued on next page*)

Continued

REAGENT or RESOURCE	SOURCE	IDENTIFIER
RT4	ECACC	RRID: CVCL_0036
T24	ECACC	RRID: CVCL_0554
Oligonucleotides		
Anti-METTL3 sgRNA1 5′-AGACTAGGATGTCGGACACG-3′	Sigma-Aldrich	N/A
Anti-METTL3 sgRNA2 5′-CTGGTGGCCCTAAGCCCAGC-3′	Sigma-Aldrich	N/A
Anti-METTL3 sgRNA3 5′-ATGCTGACCATTCCAAGCTC-3′	Sigma-Aldrich	N/A
Anti-METTL3 sgRNA4 5′-AAGTGCAAGAATTCTGTGAC-3′	Sigma-Aldrich	N/A
Non-targeting scramble sgRNA 5′-GCTGACGGCGAGCTTTAGGC-3′	Sigma-Aldrich	N/A
qPCR forward primer for METTL3 5′-CAGGCTCAACATACCCGTACT-3′	Sigma-Aldrich	N/A
qPCR reverse primer for METTL3 5′-ACATTCTCTCCCCAACTCCA-3′	Sigma-Aldrich	N/A
qPCR forward primer for CALM2 5′-GAGCGAGCTGAGTGGTTGTG-3′	Sigma-Aldrich	N/A
qPCR reverse primer for CALM2 5′-AGTCAGTTGGTCAGCCATGCT-3′	Sigma-Aldrich	N/A
Recombinant DNA		
psPAX2	psPAX2 was a gift from Didier Trono	RRID: Addgene_12260
pMD2.G	pMD2.G was a gift from Didier Trono	RRID: Addgene_12259
TLCV2	Barger et al.[32]	RRID: Addgene_87360
Software and algorithms		
ImageJ	Schneider et al.[33]	https://imagej.nih.gov/ij/
ImageJ plugin ColonyArea	Guzmán et al.[34]	https://doi.org/10.1371/journal.pone.0092444
GraphPad Prism	GraphPad Software Inc.	Version 9
MassHunter Qualitative Analysis	Agilent	Version 10.0

RESOURCE AVAILABILITY

Lead contact

Further information and requests for resources and reagents should be directed to and will be fulfilled by the lead contact, Frank Lyko (f.lyko@dkfz.de).

Materials availability

All materials generated in this study are available from the lead contact with a completed material transfer agreement.

Data and code availability

- This paper analyzes existing, publicly available data. The accession numbers for the datasets are listed in the key resources table.
- This manuscript does not report original code.
- Any additional information required to reanalyze the data reported in this paper is available from the lead contact upon request.

EXPERIMENTAL MODEL AND STUDY PARTICIPANT DETAILS

Patients and patient samples

All urothelial carcinoma samples were obtained from patients that underwent radical cystectomy at the Department of Urology and Urosurgery at the University Hospital of Mannheim. In total, tissue samples from 108 male and 29 female Caucasian patients, with an age span ranging from 41 to 88 years, were collected. Clinicopathological characteristics for all cohorts are provided in Tables S1–S3. This study was performed in adherence to the Declaration of Helsinki, and all patients gave approval to participate in this study. Approval of the Ethics Committee II of Heidelberg University (2013-845R-MA) was obtained. FFPE sections were prepared according to standard protocol and stained with haematoxylin-eosin. FFPE sections and fresh-frozen patient tissue samples were diagnosed by an uropathologist. Tumors were characterized according to the TNM classification for bladder cancer by the Union for International Cancer Control (UICC 2017). Bladder tumors with histopathological findings other than urothelial carcinoma were excluded. For the survival analyses, patients with a follow-up time of $\leq$60 days were excluded to prevent bias due to perioperative complications.

Cell culture

The cell lines used in this work were authenticated by single nucleotide polymorphism-profiling, tested for mycoplasma and cultured based on ATCC guidelines. UROtsa (obtained from a 12-year-old female) cells were cultured in RPMI medium supplemented with 5 % FBS and 1 % penicillin/streptomycin (P/S). HEK293T (obtained from a female, age not specified), RT112/84 (obtained from a female, age not specified) and UM-UC-3 (obtained from a male, age not specified) cell lines were cultured in DMEM high glucose medium supplemented with 10 % FBS and 1 % P/S. RT4 (obtained from a 63-year-old male) and T24 (obtained from an 82-year-old female) cells were cultured in McCoy's 5A (modified) medium supplemented with 10 % FBS and 1 % P/S. All cell lines were cultivated as adherent monolayers at 37°C in a humidified incubator with an atmosphere of 5 % CO_2.

METHOD DETAILS

Establishment of conditional *METTL3* knockout cell lines

The lentivirus packaging vectors psPAX2 (Plasmid #12260) and pMD2.G (Plasmid #12259) as well as the lentivirus transfer vector TLCV2[32] (Plasmid #87360) were purchased from Addgene. sgRNA oligomers comprise the following sequences: Anti-METTL3 sgRNA1: 5′-AGACTAGGATGTCGGACACG-3′. Anti-METTL3 sgRNA2: 5′-CTGGTGGCCCTAAGCCCAGC-3′. Anti-METTL3 sgRNA3: 5′-ATGCTGACCATTCCA AGCTC-3′. Anti-METTL3 sgRNA4: 5′-AAGTGCAAGAATTCTGTGAC-3′. Non-targeting scramble sgRNA: 5′-GCTGACGGCGAGCTTTAGGC-3′. For lentivirus production, HEK293T cells were transfected with the lentiviral vectors using Lipofectamine 2000 (Thermo Fisher Scientific, Waltham, MA, USA) and incubated for 48 hours. Supernatants were then spun down and filtered (0.42 μm pore size, cellulose acetate filter). T24 and UM-UC-3 cells were incubated in the lentivirus containing filtrate for 48 hours in the presence of 10 μg/mL polybrene, and then selected in 3 μg/mL puromycin for 1 week.

Cell proliferation, clonogenicity and apoptosis assays

For all functional assays, cells were seeded and induced with 100 ng/mL doxycycline after attachment.

For cell proliferation assays using cell pools, T24 and UM-UC-3 Scr and *METTL3* knockout cells were seeded in 12-well plates with the following densities: T24 cells: 8 x 10^3 cells/well. UM-UC-3 cells: 12 x 10^3 cells/well. Cell proliferation was quantified by counting the cells using the Z1 Coulter Particle Counter (Beckman Coulter, Brea, CA, USA) for 5 consecutive days in time intervals of 24h. 24h to 96h measurements were normalized to the 0h measurement.

For cell proliferation assays using clonal cell populations, T24 and UM-UC-3 Scr and *METTL3* knockout clones were seeded in 96-well plates with the following densities: T24 cells: 750 cells/well. UM-UC-3 cells: 1500 cells/well. Cell proliferation was quantified by Cell Titer-Glo (Promega) measurements for 5 consecutive days in time intervals of 24h. 24h to 96h measurements were normalized to the 0h measurement.

For clonogenicity assays, T24 and UM-UC-3 Scr and *METTL3* knockout cells were seeded in 6-well plates with the following densities: T24 cells: 500 cells/well. UM-UC-3 cells: 1000 cells/well. Then, cells were incubated for 1.5 weeks and fixed with ice-cold methanol for 10 min. Staining was conducted using

a 0.5 % crystal violet solution for 10 min at room temperature. Colonies were counted using the ImageJ plugin "ColonyArea".[34]

For apoptosis assays, T24 and UM-UC-3 Scr and *METTL3* knockout cells were seeded in 96-well plates with 10^4 cells/well. Caspase activity was quantified by the Caspase-Glo 3/7 Assay kit (Promega) 48h after knockout induction. Also, a Cell Titer-Glo (Promega) measurement was conducted to determine the number of seeded cells for normalization.

Inhibitor response assay

UROtsa, RT4, RT112/84, T24 and UM-UC-3 cells were seeded in 96-well plates with the following densities: UROtsa: 4 x 10^3 cells/well, RT4: 5 x 10^3 cells/well, RT112/84: 3.5 x 10^3 cells/well, T24: 2 x 10^3 cells/well, UM-UC-3: 2.5 x 10^3 cells/well. Considering the cell lines' different proliferation rates, different amounts of cells were seeded to obtain similar confluency for starting the treatment. After attachment, a Cell Titer-Glo (Promega) measurement was conducted to determine the number of seeded cells for normalization. Cells were then treated for 72h with DMSO or the indicated concentrations (0.01 – 200 μM) of the METTL3 inhibitor STM2457 (MedChemExpress, Princeton, NJ, USA). Cell viability after 72h was quantified by Cell Titer-Glo measurements (Promega).

Western blotting

T24 and UM-UC-3 Scr and *METTL3* knockout cells were cultured in 6-well plates. After attachment, cells were treated with 100 ng/mL doxycycline to induce *METTL3* knockout. 24h after knockout induction, cells were lysed in a buffer containing 20 mM Tris-HCl (pH 7.5), 150 mM NaCl, 1 mM EDTA and 1 % Triton-X-100 supplemented with the Complete Protease Inhibitor Cocktail (Roche, Basel, Switzerland) and proteins separated by SDS-PAGE. Proteins were transferred to nitrocellulose membranes using a Trans-Blot Turbo Transfer System (Bio-Rad, Hercules, CA, USA), and membranes blocked in blocking buffer (PBS-T containing 5 % (w/v) milk powder) for 1h at room temperature. Primary antibody incubation was performed overnight at 4°C using the following antibodies: Anti-METTL3 (15073-1-AP, Proteintech, Rosemont, IL, USA c = 1:1000), anti-β-Actin (sc-47778, Santa Cruz Biotechnology, Dallas, TX, USA, c = 1:1000) and anti-Cas9 (A-9000, Epigentek, Farmingdale, NY, USA, c = 1:1000). Secondary antibody incubation occurred for 1h at room temperature. Membranes were imaged using the Immobilon Western Chemiluminescent HRP Substrate (Merck Millipore, Burlington, MA, USA) and signals detected using a M6 ECL Chemostar fluorescence imaging system (Intas, Göttingen, Germany). Images were finally analyzed by a ChemoStar V60+ device and ImageJ software.[33]

Immunohistochemistry

Paraffin tissue slides were dewaxed and rehydrated, followed by antigen retrieval through microwave-based heating. After blocking with fetal bovine serum, slides were incubated with a primary anti-METTL3 antibody (ab195352, Abcam, Cambridge, United Kingdom, c = 1:500) overnight. The slides were then incubated with a secondary anti-rabbit HRP antibody for 1h at room temperature. Immunoreactive scores (IRS) were used to quantify the acquired images.[35]

Liquid chromatography-tandem mass spectrometry (LC-MS/MS) for the analysis of m^6A mRNA methylation levels

T24 and UM-UC-3 Scr and *METTL3* knockout cells were cultured in 10 cm dishes. After attachment, cells were treated with 100 ng/mL doxycycline to induce *METTL3* knockout. Total RNA was isolated after the indicated time points (24h – 1 week) using Trizol (Thermo Fisher Scientific). Fresh-frozen patient tissue samples were homogenized by disruption using the TissueRuptor (Qiagen, Hilden, Germany) and total RNA isolated with Trizol (Thermo Fisher Scientific). mRNA fractions from cell and patient samples were isolated from total RNA by using the Dynabeads mRNA purification kit (Thermo Fisher Scientific), following the manufacturer's instructions.

400 ng of total RNA or 200 ng of mRNA per sample was digested to nucleosides using 0.6 U nuclease P1 from *P. citrinum* (Sigma-Aldrich, St. Louis, MO, USA), 0.2 U snake venom phosphodiesterase from *C. adamanteus* (Worthington, Lakewood, NJ, USA), 0.2 U bovine intestine phosphatase (Sigma-Aldrich), 10 U benzonase (Sigma-Aldrich), 200 ng Pentostatin (Sigma-Aldrich) and 500 ng Tetrahydrouridine (Merck-Millipore) in 5 mM Tris (pH 8) and 1 mM magnesium chloride for 2h at 37°C. 100 ng of digested total

RNA or 50 ng of mRNA was mixed with 25 ng of internal standard (13C stable isotope-labeled nucleosides from *S. cerevisiae*) and subjected to LC-MS/MS analysis (Agilent 1260 Infinity system in combination with an Agilent 6470 Triple Quadrupole mass spectrometer equipped with an electrospray ion source). The solvents consisted of 5 mM ammonium acetate buffer (pH 5.3, adjusted with acetic acid; solvent A) and LC-MS grade acetonitrile (solvent B; Honeywell, Charlotte, NC, USA). A C18 reverse HPLC column (SynergiTM 4 μM particle size, 80 Å pore size, 250 × 2.0 mm; Phenomenex, Torrance, CA, USA) was used at a temperature of 35°C. The compounds were eluted with a constant flow rate of 0.35 mL/min and a linear gradient of 0 – 8 % solvent B over 10 min, followed by 8 – 40 % solvent B over 10 min was applied. Initial conditions were regenerated with 100 % solvent A for 10 min. Adenosine was detected photometrically at 254 nm via a diode array detector (DAD). The following mass parameters were used: gas temperature 300°C, gas flow 7 L/min, nebulizer pressure 60 psi, sheath gas temperature 400°C, sheath gas flow 12 L/min, capillary voltage 3000 V, nozzle voltage 0 V. The MS was operated in the positive ion mode using Agilent MassHunter software in the dynamic MRM (multiple reaction monitoring) mode. For absolute quantification, internal calibration was applied as described in Thüring et al.[36] Briefly, absolute quantification was performed by using external calibration solutions. Calibration solutions with concentrations of 0.1, 0.5, 1, 5, 10, 50, 100 and 500 nM for MS/MS-detected modifications were prepared, each containing equal amounts of internal standard. By injection of 10 μL of each dilution, a calibration in a range from 1-5000 fmol was achieved. The mass chromatograms of each modified nucleoside and its 13C-labeled counterparts were extracted, and peaks were integrated to obtain the peak areas. For calibration curves, the ratio of 12C and 13C peak areas of the modification were plotted to the amount of 12C reference nucleoside. The slope of the linear fit was calculated. For quantitative analysis of the RNA samples, each sample was spiked with the same amount of internal standard as used for the calibration curves. The amount of modified nucleoside was calculated by dividing the ratio of 12C and 13C peak areas of the modification by the slope of the linear fit of the respective modification. In a last step, the amount of the modified nucleoside was normalized to the amount of adenosine, based on the slope of a recorded calibration curve. Therefore, calibration solutions with concentrations of 0.1, 1, 10 and 100 μM were prepared and a calibration in a range from 0.5-500 pmol was achieved by injection of 5 μL of each dilution.

Quantitative real-time PCR for METTL3 expression analysis

To determine METTL3 expression levels in the UKMA validation cohort, tumorous parts from FFPE slides were identified for RNA extraction. A 10-μm thick section per sample was used for RNA isolation with the XTRAKT FFPE kit (Stratifyer, Köln, Germany). cDNA synthesis was performed using the SuperScript III First-Strand Synthesis System (Thermo Fisher Scientific). Quantitative real-time PCR was performed using the Mesa Green qPCR MasterMix Plus for SYBR (Eurogentec, Seraing, Belgium) and 0.3 mM forward and reverse primers for METTL3 (forward 5′-CAGGCTCAACATACCCGTACT-3′, reverse 5′-ACATTCTCTCCCC AACTCCA-3′) and CALM2 as a housekeeping gene control (forward 5′-GAGCGAGCTGAGTGGTTGTG-3′, reverse 5′-AGTCAGTTGGTCAGCCATGCT-3′. Expression levels were measured in triplicates and analyzed using the ΔΔCt-method. Normalization was performed using the housekeeping gene CALM2.

In-silico data analysis

Data analysis of the Cancer Genome Atlas (TCGA) was performed using the public available normalised and log2-transformed RNA-Seq data (HiSeq) of the urothelial carcinoma dataset (BLCA). Expression data were requested and downloaded via the Xena browser (www.xenabrowser.net). The completion of the clinicopathological data was done via the cBioPortal for Cancer Genomics (https://www.cbioportal.org/). Patients lacking clinical or expression data were excluded. Final TCGA data analysis was performed on 425 samples, 406 muscle invasive urothelial carcinomas and 19 para-tumoral bladder tissues.

DepMap analysis

Dependency probability scores were obtained from the DepMap Public 22Q2 CRISPR gene dependency dataset (https://depmap.org/portal/download/all/). The probability that a CRISPR/Cas9-mediated gene knockout inhibits cell proliferation or leads to cell death is expressed as a gene dependency probability score. A cell line is considered dependent on a gene if its dependency probability score is greater than 0.5. Dependency probability scores were extracted from the datasets and plotted in order to investigate *METTL3*, *POLR2F*, and *DNMT2/TRDMT1* dependencies in UCB and all other cell lines.

QUANTIFICATION AND STATISTICAL ANALYSIS

If not stated otherwise, cell culture experiments were conducted in biological and technical triplicates. Data are represented as mean ± standard deviation (SD). All statistical analyses were performed using Prism (GraphPad Software Inc., La Jolla, CA, USA). Cell proliferation assays were analyzed by two-way analysis of variance. Colony formation assays, apoptosis assays, and LC-MS/MS measurements were analyzed by the two-tailed Student's t-test when comparing cell pools resp. one-way analysis of variance when comparing clonal cell populations. DepMap data were analyzed by the Mann-Whitney-U test. Western blot experiments with STM2457-treated T24 and UM-UC-3 cells were analyzed by one-way analysis of variance. METTL3 expression and m^6A mRNA methylation in patient samples were analyzed by the Mann-Whitney-U test or chi-square-test as indicated. Expression data from the TCGA dataset of further m^6A writer complex components were analyzed by the Mann-Whitney-U test. Kaplan-Meier plots were analyzed by the log-rank test and complemented by univariable Cox regression analyses. Statistical details of all experiments can be found in the results section of the manuscript and in the corresponding figure legends. A p-value of <0.05 was considered significant in all analyses.